

The K-Band Galaxy Luminosity Function¹²

C. S. Kochanek, M. A. Pahre³, E. E. Falco, J. P. Huchra, J. Mader,
Harvard-Smithsonian Center for Astrophysics
60 Garden Street
Cambridge, MA 02138
ckochanek, mpahre, efalco, jhuchra, jmader@cfa

T.H Jarrett, T. Chester, R. Cutri,
Infrared Processing and Analysis Center, MS 100-22,
California Institute of Technology
Pasadena, CA 91125
jarrett, tchester, roc@ipac.caltech.edu

and S.E. Schneider
Department of Astronomy
University of Massachusetts
Amherst, MA 01003
schneider@messier.astro.umass.edu

ABSTRACT

We measured the K-band luminosity function using a complete sample of 4192 morphologically-typed 2MASS galaxies with $\mu_{K_s} = 20$ mag/arcsec² isophotal magnitudes $7 < K_{20} < 11.25$ mag spread over 2.12 str. Early-type ($T \leq -0.5$) and late-type ($T > -0.5$) galaxies have similarly shaped luminosity functions, $\alpha_e = -0.92 \pm 0.10$ and $\alpha_l = -0.87 \pm 0.09$. The early-type galaxies are brighter, $M_{*e} = -23.53 \pm 0.06$ mag compared to $M_{*l} = -22.98 \pm 0.06$ mag, but less numerous, $n_{*e} = (0.45 \pm 0.06) \times 10^{-2} h^3 \text{ Mpc}^{-3}$ compared to $n_{*l} = (1.01 \pm 0.13) \times 10^{-2} h^3 \text{ Mpc}^{-3}$ for $H_0 = 100h \text{ km s}^{-1} \text{ Mpc}^{-1}$, such that the late-type galaxies slightly dominate the K-band luminosity density, $j_{\text{late}}/j_{\text{early}} = 1.17 \pm 0.12$. Our morphological classifications are internally consistent, consistent with previous classifications and lead to luminosity functions unaffected by the estimated uncertainties in the classifications. These luminosity functions accurately predict the K-band number counts and redshift distributions for $K \lesssim 18$ mag, beyond which the results depend on galaxy evolution and merger histories.

¹This publication makes use of data products from the Two Micron All Sky Survey (2MASS), which is a joint project of the University of Massachusetts and the Infrared Processing and Analysis Center/California Institute of Technology, funded by the National Aeronautics and Space Administration and the National Science Foundation.

²This research has made use of the NASA/IPAC Extragalactic Database (NED) which is operated by the Jet Propulsion Laboratory, California Institute of Technology, under contract with the National Aeronautics and Space Administration.

³Hubble Fellow.

Subject headings: cosmology: observations – galaxies: distances and redshifts – galaxies: luminosity function – surveys

1. Introduction

The luminosity function (LF) of galaxies, its parameters, dependence on galaxy type, and evolution are fundamental to observational cosmology and the theory of galaxy formation. Most existing estimates of the luminosity function are based on redshift surveys of galaxies selected from blue photographic plates (CfA/CfA2, Davis & Huchra 1982, de Lapparent, Geller & Huchra 1989, Geller & Huchra 1989, Marzke et al. 1994ab; SSRS2 da Costa et al. 1994, 1998, Marzke et al. 1998; APM, Loveday et al. 1992; ESO Slice, Vettolani et al. 1997, Zucca et al. 1997; 2dFGRS Folkes et al. 1999, Slonim et al. 2000). The luminosity function derivations are usually based on samples of ~ 5000 galaxies. Blue surveys emphasize galaxies with active star formation, are sensitive to both Galactic and internal extinction, and those based on photographic plates usually have large photometric uncertainties (0.2–0.4 mag). Deep, blue-selected surveys must also include strong, type-dependent K-corrections. The only ongoing blue survey is the 2dFGRS of 250,000 galaxies.

Most recent surveys have shifted to selecting galaxies in the red, which somewhat reduces the effects of extinction and leads to samples less influenced by recent star formation. The Century Survey (Geller et al. 1997) used objects selected from red photographic plates with the photometry recalibrated by R_c -band drift scans, while the Las Campanas Redshift Survey (hereafter the LCRS, Shectman et al. 1996, Lin et al., 1996, Bromley et al. 1998) selected the galaxies from Gunn r-band drift scans calibrated to approximate Kron-Cousins R_c . The Sloan Digital Sky Survey (SDSS) will obtain a surface-brightness limited sample to $r' = 17.7$ mag with approximately 10^6 galaxies (see York et al. 2000).

Infrared galaxy surveys have smaller systematic uncertainties than optical galaxy surveys. They are almost immune to both Galactic and internal extinction, and the K-corrections and luminosity per unit stellar mass are nearly independent of galaxy type (e.g. Cowie et al. 1994, Gavazzi, Pierini & Boselli 1996). The determination of infrared luminosity functions has proceeded slowly, however, because of the difficulty of obtaining large complete samples. Mobasher, Sharples & Ellis (1993) and Loveday (2000) obtained infrared photometry of optically-selected galaxies to estimate the infrared LF. Glazebrook et al. (1994, 1995), Gardner et al. (1997) and Szokoly et al. (1998) used relatively deep IR surveys of small regions, where the faintness of the targets makes it difficult to obtain redshifts of the full sample. De Propris et al. (1998) and Andreon & Pello (2000) have also estimated the infrared luminosity function by constructing volume limited samples of galaxies in the Coma cluster. The resulting samples are typically 10 times smaller than published optical samples (~ 500 rather than ~ 5000 galaxies).

The 2MASS project (Skrutskie et al. 1997) is obtaining a complete infrared map of the sky, with a limiting magnitude for its galaxy catalog of $K_s \simeq 13.5$ mag. Since 2MASS overlaps the existing optical surveys, it is easy to rapidly generate large, complete infrared redshift surveys. In

this paper we discuss an infrared redshift survey overlapping the CfA2 survey and the updated Zwicky catalog (UZC, Falco et al. 1999). To a magnitude limit of $K_{20} \leq 11.25$ mag, $\sim 90\%$ of the galaxies already have redshifts and the remainder were obtained as part of our redshift survey. For the first time we can derive infrared luminosity functions from samples of comparable size to that of the published optical luminosity functions. In §2 we discuss the sample selection, in §3 we derive the luminosity function by galaxy type, and in §4 we compare the results to other estimates of the luminosity function. In §5 we use our luminosity functions to predict the properties of fainter infrared galaxy samples, and in §6 we summarize our results.

2. Sample Selection and Data

We selected 4353 targets from the 2MASS Second Incremental Release Catalog of Extended Sources using the default K_s -band survey magnitudes, K_{20} , which is the magnitude inside the circular isophote corresponding to a surface brightness of $\mu_{K_s} = 20$ mag/arcsec² (see Jarrett et al. 2000a). The K_{20} isophotal magnitude is 10–20% less than the total flux, depending on the galaxy type. We selected all extended sources with $7 \leq K_{20} \leq 11.25$ mag, $\delta \geq 11^\circ$ (J2000) and $|b| \geq 20^\circ$, modulated by the actual sky coverage of the release (see Figure 1). Although there is no exact correspondence to optical redshift surveys because of the wide range of optical to infrared galaxy colors, our magnitude limit roughly corresponds to $B \lesssim 15$ mag or $R_c \lesssim 14$ mag. The effective optical limits are deeper for red early-type galaxies and shallower for blue late-type galaxies. Objects which were not galaxies (artifacts, double stars, planetary nebula, ...) were removed from the sample by inspection of the 2MASS data flags and images, the NED databases and digitized POSS-II^{4 5} images of the targets, leaving a sample of 4192 galaxies. We determined the survey area by integrating over the survey scans (the scans are $8'5 \times 6^\circ$). Note that the lower boundary of the scanned region actually lies between 11.5° and 12° in Declination. The scanned regions inside the angular boundaries cover $\Delta\Omega = 2.12$ str which is $2/3$ of the area inside the boundaries. The uncertainties in the survey area are less than 5% but they are difficult to estimate precisely because they depend on the detailed treatment of galaxies near the edges. A few percent of the area is also masked by bright stars.

Since the survey region overlaps the CfA2 redshift survey (Geller & Huchra 1989) and the UZC (Falco et al. 1999), almost all the galaxies in the sample had known redshifts. We based our redshift catalog on ZCAT (Huchra et al. 1992, <http://cfa-www.harvard.edu/~huchra/zcat>), but checked the redshifts against the UZC reanalysis of the CfA/CfA2 redshift survey and reconciled or corrected any significant disagreements between the two redshift catalogs. The galaxies

⁴The Second Palomar Observatory Sky Survey (POSS-II) was made by the California Institute of Technology with funds from the National Science Foundation, the National Geographic Society, the Sloan Foundation, the Samuel Oschin Foundation, and the Eastman Kodak Corporation. The Oschin Schmidt Telescope is operated by the California Institute of Technology and Palomar Observatory.

⁵The Digitized Sky Surveys were produced at the Space Telescope Science Institute under U.S. Government grant NAG W-2166. The images of these surveys are based on photographic data obtained using the Oschin Schmidt Telescope on Palomar Mountain and the UK Schmidt Telescope. The plates were processed into the present compressed digital form with the permission of these institutions.

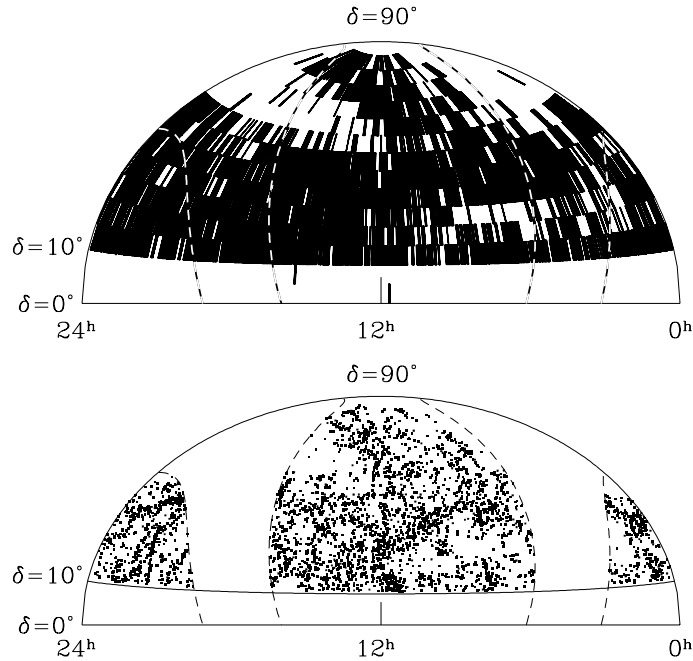


Fig. 1.— Aitoff projections of the 2MASS scan coverage (top) and the sample galaxies (bottom) in equatorial coordinates. The dashed lines show the $|b| \geq 20^\circ$ Galactic latitude limits and the solid line shows the lower declination limit at $\delta \geq 10^\circ$.

lacking redshifts were primarily elliptical galaxies whose Zwicky magnitudes were fainter than the UZC magnitude limit and galaxies outside the CfA survey area but inside our Galactic latitude limits. We obtained the missing redshifts using the FLWO Tillinghast 1.5m telescope, the FAST spectrograph (Fabricant et al. 1998), and standard reduction procedures (Kurtz & Mink 1998). Figure 1 shows an Aitoff projection of the galaxy sample.

The morphological types of the galaxies are important for studies of galaxy evolution (e.g. Lilly et al. 1995) and the differences between galaxy environments (e.g. Dressler 1980). Our galaxies are relatively nearby, which allows us to morphologically classify the galaxies. Of the 4192 galaxies, only 1673 have unambiguous types in the RC3 catalog (de Vaucouleurs et al. 1976). Each galaxy was visually classified by at least two of the authors (EEF, JPH, CSK and MAP did the classification) using digitized POSS-II images (POSS-I⁶ for the small fraction where POSS-II was unavailable). The galaxies were assigned to the classifiers randomly and without information on the classifications from RC3 or the other classifiers. We did not, in general, make use of the full range of fine distinctions in the T-type scale for early-type galaxies and very late-type galaxies. Most classifiers used E, E/S0 and S0 for early-type galaxies (rather than cE, E, E+, S0–, S0

⁶The National Geographic Society-Palomar Observatory Sky Atlas (POSS-I) was made by the California Institute of Technology with grants from the National Geographic Society.

and S0+), and the very late-type galaxy classifications (Sd, Sdm, Sm and Im) were not applied uniformly. T-types are more finely grained than we ultimately require, and our classifications will be internally consistent viewed as the sequence E, E/S0, S0, S0/a, Sa, Sab, Sb, Sbc, Sc, Scd, Sd+later. Flags were added for bars (“B”), possible bars (“X”), peculiar morphologies (“pec”) and evidence for overlapping or interacting neighboring galaxies (“int”). Our philosophy for interacting and peculiar galaxies was to assign our best estimate of the “intrinsic” morphology rather than classifying based on the transient structures created by the interaction. The flags were set whenever one classifier assigned it to the galaxy, and they should be regarded as indicative but not as statistically reliable as the galaxy types because they were not subject to the same level of inspection.

Once the preliminary classifications were complete, we reconsidered the galaxies with classification ranges covering more than 4 T-types. These galaxies were reclassified by all four classifiers with knowledge of all the classifications. The worst cases were dominated by interacting galaxies, galaxies with odd star formation patterns, galaxies classed as “Irr” meaning “peculiar” rather than “Im” ($T = 10$) in RC3, and the fine grained nature of the early and very late T-types. Galaxies with type ranges greater than 5 T-types were individually discussed. A limited number of RC3 classifications, largely galaxies classified as “Irr”, were deleted. The final classification was the average T-type of all the classifications. Figure 2 compares our internal classifications and the RC3 classifications for the galaxies in both samples, as a function of the RC3 T-type. The average difference between the RC3 T-types and our average T-types is 0.01 with a dispersion of 1.6, while the average differences between the individual classifiers and RC3 ranged from -0.28 to $+0.24$ with dispersions of 1.8 T-types. These statistics closely resemble the results found by Naim et al. (1995ab) when comparing morphological classifications of a range of observers and a neural network, and the biases and scatter are dominated by the very early-type and very late-type galaxies where we had not attempted to closely recreate the RC3 classification system. We will divide our sample into early-type and late-type galaxies at $T = -0.5$, so our systematic uncertainties will be dominated by the classification errors for S0, S0/a and Sa galaxies (see Figure 2). The galaxy sample is presented in Table 1.

The conversion from apparent to absolute magnitude,

$$M_K = K_{20} - 5 \log(D_L(z)/r_0) - R_K E(B - V) - k(z) \quad (1)$$

has terms for the distance modulus, Galactic extinction $A_K = R_K E(B - V)$ and the K-correction, $k(z)$. The luminosity distance is $D_L(z) = 6000h^{-1}(1 + z - (1 + z)^{1/2})$ Mpc for Hubble constant $H_0 = 100h$ km s $^{-1}$ Mpc $^{-1}$ and assuming $\Omega_0 = 1$, although the particular cosmological model is unimportant given our median redshift of $cz = 7000$ km s $^{-1}$. The galaxy magnitudes were corrected for Galactic extinction using the extinction maps of Schlegel, Finkbeiner & Davis (1998) and an extinction coefficient of $R_K = 0.35$ where $A_K = E(B - V)R_K$ (Cardelli, Clayton & Mathis 1989). The Galactic extinction was less than $E(B - V) = 0.03$ mag (0.14 mag) for 50% (95%) of the sample, and the maximum extinction was $E(B - V) = 0.64$ mag. Thus, while we include the extinction corrections, they are of little importance. The K_s -band K-correction of $k(z) = -6.0 \log(1 + z)$ is negative, independent of galaxy type, and valid for $z \lesssim 0.25$ (based on the Worthey 1994 models). Unlike most previous estimates of the local luminosity function, our intrinsic photometric errors make a negligible contribution to the uncertainties in the LF

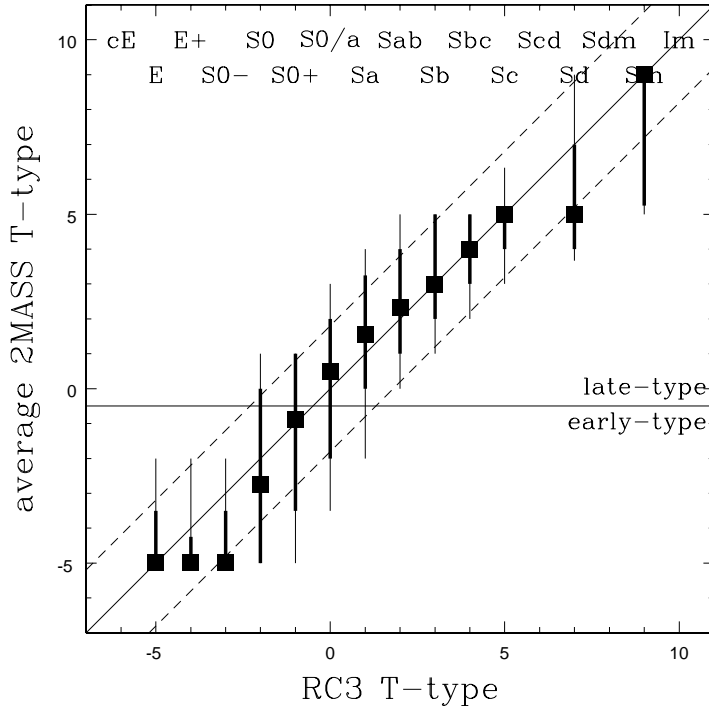


Fig. 2.— We show the median (point), 1σ range (heavy error bars, 68.3% of galaxies) and 2σ range (light error bars, 95.4% of galaxies) of our classifications as a function of the RC3 T-type for the 2MASS galaxies found in the RC3 catalog. The dashed lines show the typical 1.8 dispersion in T-type classifications found by Naim et al. (1995), and the horizontal line shows where we break the sample into early-type and late-type galaxies for determining the luminosity function. Most of the 2MASS classifiers did not use the full range of T-types available for early-type galaxies (S0 and earlier) and extremely late-type galaxies (Sd and later), leading to the differences at the edges of the T-type scale. These differences have no effect on our division of the sample into early and late-type galaxies.

calculation. The median error in K_{20} for our sample is 0.03 mag and 90% of the galaxies have errors less than 0.04 mag. These estimates are verified through repeated scans of several areas on well-separated nights (Jarrett et al. 2000b). Our isophotal magnitudes will have type-dependent differences from integrated magnitudes.

Given the low redshift of our sample, we need to include corrections for peculiar velocities in the redshift estimates. We corrected the heliocentric radial velocities using the local flow model of Tonry et al. (2000). While the Tonry et al. (2000) model is computed using a different cosmology and Hubble constant, we use it only as means of estimating the peculiar velocity corresponding to a given heliocentric velocity. For our standard analysis we restrict the sample to galaxies with corrected velocities exceeding $cz > 2000 \text{ km s}^{-1}$. This velocity limit eliminates the Virgo cluster from the sample at the price of a significant reduction in the luminosity range of the galaxies in the sample. We also analyzed the sample down to $cz > 1000 \text{ km s}^{-1}$, which includes the Virgo

cluster and extends the luminosity function determination to significantly fainter magnitudes at the price of including galaxies whose luminosities include a significant dependence on the local flow corrections.

3. The Luminosity Function

We used the standard parametric (Sandage, Tammann & Yahil 1978, hereafter STY) and non-parametric stepwise maximum-likelihood (SWML, Efstathiou, Ellis & Peterson 1988) methods for determining the shape of the luminosity function, and the Davis & Huchra (1982) minimum variance estimator for determining the absolute number density. These methods are almost universally used for galaxy luminosity function determinations (see Lin et al. 1996 and references therein). The completeness of the sample and the negligible magnitude errors considerably simplify the analysis over most recent studies. We used the Schechter (1976) parametric model,

$$\frac{dn}{dL} = \frac{n_*}{L_*} \left(\frac{L}{L_*} \right)^\alpha \exp(-L/L_*) \quad (2)$$

for the STY method fits. For our standard fits we estimated the luminosity function using galaxies with flow-corrected velocities $cz > 2000 \text{ km s}^{-1}$, which excludes the bulk of the Virgo cluster and restricts us to galaxies with absolute magnitudes brighter than $M_K < -20.2 \text{ mag}$. The density normalization was determined using the velocity range $2000 \text{ km s}^{-1} < cz < 14000 \text{ km s}^{-1}$, the absolute magnitude range $-25 \text{ mag} < M_K < -22 \text{ mag}$. We set the second moment of the correlation function, needed to estimate the effects of sample variance on the galaxy density, to $J_3 = 10^4 (h^{-1} \text{Mpc})^3$ (Lin et al. 1996). We also show fits using galaxies with $cz > 1000 \text{ km s}^{-1}$, which extends our absolute magnitude range to $M_K < -18.7 \text{ mag}$ at the price of increased sensitivity to errors in the velocity corrections. We have 3878 (4096) galaxies left in the sample with the velocity limit $cz > 2000 \text{ km s}^{-1}$ (1000 km s^{-1}). Our redshift and magnitude limits also remove almost all the large galaxies ($\gtrsim 2'$) which have unreliable magnitude estimates in the 2MASS Second Incremental Release. The luminosity function estimation software was tested using synthetic catalogs drawn from a Poisson spatial distribution of galaxies selected from Schechter luminosity functions. The SWML binned luminosity functions are presented in Table 2 and the Schechter function model luminosity functions are presented in Table 3.

Figure 3 shows luminosity functions for the full sample, the early-type galaxies and the late-type galaxies using the two different estimation methods. Early-type galaxies were defined to be all galaxies with $T \leq -0.5$ so that S0/a galaxies are counted as late-type galaxies and S0+ galaxies are counted as early-type galaxies. Because the distributions of the T-type classifications are somewhat quantized, the exact location of the boundary between $-1 < T < 0$ has little effect on the results. The luminosity functions found for the $cz > 2000 \text{ km s}^{-1}$ and $cz > 1000 \text{ km s}^{-1}$ samples are mutually consistent. Figure 4 shows the likelihood contours for the Schechter function α and M_* parameters as compared to earlier derivations of the infrared luminosity functions. Note that the early-type and late-type luminosity functions have similar shapes, as was also found in the CfA (Marzke et al. 1994b) and SSRS2 (Marzke et al. 1998) morphologically classified luminosity functions. The total luminosity function is steeper than those of the individual types ($\alpha = -1.09 \pm 0.06$ rather than $\alpha = -0.87 \pm 0.09$ or -0.92 ± 0.10) because adding the fainter,

more numerous late-type galaxies to the early-type galaxies makes the summed luminosity function steeper than either of the components. The values of α and M_* are strongly correlated, with a dimensionless covariance of $C_{\alpha M_*}/(C_{\alpha\alpha}C_{M_*M_*})^{1/2} = 0.85$ for all three $cz > 2000$ km s⁻¹ luminosity functions, as we would expect from the shapes of the likelihood contours in Figure 4. The uncertainties in the galaxy density have similar contributions from sampling errors and changes correlated with α and M_* ⁷

We also explored the effects of classification errors on the results. We first examined the effects of simple classification errors using Monte Carlo resampling. We randomly selected a new galaxy sample (bootstrap resampling with replacement) including Poisson variations in the total number of galaxies. For each galaxy, we added a 1.8 T-type Gaussian deviate to its classification before dividing the sample into early-type and late-type galaxy subsamples. This random dispersion is a little larger than the 1.6 T-type dispersion between our internal classifications and RC3, but matches the dispersion in the morphological classification experiments conducted by Naim et al. (1995ab). The results after repeating the process 100 times are summarized in Table 3, where we present the average parameters and their dispersions. These uncertainty estimates will underestimate the uncertainties in the absolute density normalization because they include only the Poisson variance in the expected number of galaxies without the sample variance due to our survey volume and larger scale structure. Aside from the sample variance, the parameter errors and correlations estimated by these bootstrap calculations should be more statistically reliable than those estimated from the likelihood function. The results are stable to these statistical errors, since the Schechter function parameters and their bootstrap uncertainties are consistent with the simpler maximum likelihood estimates. As we discuss in Kochanek, Pahre & Falco (2000), luminosity functions are not stable to even small, random classification uncertainties when the luminosity function shape depends strongly on the type (as is found in spectrally-typed luminosity functions like ESP, LCRS and 2dFGRS). We computed the luminosity density ratio, $j_{late}/j_{early} = 1.17 \pm 0.12$, using the bootstrap calculations since they include the full variable covariances and classification uncertainties. The early-type and late-type galaxies have nearly equal luminosity densities, although the exact ratio and the true uncertainties will differ from this estimate because of the type-dependent corrections between isophotal and total magnitudes.

Next we explored the sensitivity of the results to shifts in the boundary between early-type and late-type galaxies. In our standard LF determination we set the boundary at $T = -0.5$ so that the S0/a galaxies (type $T = 0$) are counted as late-type galaxies. In Table 3 we show the results of shifting the boundary for early-type galaxies to $T \leq -1.5$ (S0 is the first early-type), -0.5 (our standard LF, with S0+ is the first early-type), 0.5 (S0/a is the first early-type), and 1.5 (Sa is the first early-type). The parameters K_* and α are insensitive to the boundary shifts, while the comoving density n_* follows the changes in the relative numbers of galaxies.

Figure 4 and Table 4 compare our Schechter parameter estimates to previous results for the total infrared luminosity function from Mobasher et al. (1993), Glazebrook et al. (1995), Gardner et al. (1997), Szokoly et al. (1998), and Loveday (2000). The sample sizes of these surveys are

⁷The value of n_* changes with α and M_* as $n_* = 0.45 - 0.25\Delta\alpha + 0.77\Delta M_*$ for the early-type galaxies and as $n_* = 1.01 - 0.92\Delta\alpha + 2.44\Delta M_*$ for the late-type galaxies where $\Delta\alpha$ and ΔM_* are the changes in α and M_* from the maximum likelihood solutions and n_* is in units of $10^{-2}h^3/\text{Mpc}^3$.

so much smaller that their statistical uncertainties dominate any comparison to our results. All the results are mutually consistent given the uncertainties, with the exception of the anomalously high density normalization for the Glazebrook et al. (1995) survey. The uncertainties in the Coma luminosity function estimates by de Propris et al. (1988) and Andreon & Pello (2000) are significantly larger than for these field surveys.

4. Comparison to Optical Luminosity Functions

Our infrared luminosity functions are the first large enough to compare directly to the results of recent estimates of the luminosity function from optical redshift surveys, which are summarized in Table 5. The optical luminosity functions, particularly those divided by galaxy type, show inconsistencies in their magnitude scales, shapes and density normalizations that are significantly larger than their formal uncertainties. In Kochanek et al. (2000) we show that the luminosity functions defined by spectral types using small aperture fiber spectrographs (LCRS, ESP, and by extension 2dFGRS and SDSS) have internally inconsistent type definitions which can severely bias the shapes of the derived luminosity functions. In essence, the small spectral apertures sample a varying fraction of the bulge and the disk of spiral galaxies, leading to flux and luminosity dependent biases between the true and measured spectral types of the galaxies. Local, bright, morphologically-typed surveys (this sample, CfA and SSRS2) and large aperture spectrally typed surveys (APM survey by spectral type) appear to have self-consistent type definitions and similarly shaped luminosity functions for both early and late-type galaxies. Differences in the surface brightness selection effects of the surveys can also lead to differences in the shapes of the luminosity functions (e.g. Disney 1976, Huchra 1999, Cross et al. 2000).

The luminosity scales (L_* or M_*) of the optical surveys differ by more than can be explained by any statistical uncertainties even after including the strong covariances between α and M_* in Schechter function models of the luminosity function. For example, the value of M_* found for the CfA survey (Marzke et al. 1994ab) is 0.75 mag fainter than the other blue-selected surveys (APM, ESP, SSRS2 and 2dFGRS). The current 2MASS catalogs overlap many of the optical surveys, which allows us to calculate the extinction and K-corrected average “color” $\langle m - K_{20} \rangle$ between the optical survey and the 2MASS survey. This “color” includes both the true color difference of the galaxies and terms due to the different apertures used by the surveys to define their magnitudes. Since the intrinsic colors and the 2MASS magnitudes do not depend on the properties of the optical surveys, we can use the color differences between the surveys to test for differences in magnitude definitions and type assignments. We can estimate the average colors for the APM, CfA, LCRS and SSRS2 surveys, and we present the results in Table 5. As we would expect, later-type galaxies are bluer than early-type galaxies, but the color differences can be significantly smaller than the width of the color distribution. For example, the LCRS emission line and non-emission line samples (Lin et al. 1996) have a color differences of only 0.15 mag but a much larger dispersion in the colors of each type. The depth of the 2MASS survey is not well matched to that of the LCRS survey, so our color estimate is dominated by the bright LCRS galaxies (the 2MASS galaxy magnitude limit of $K_s \simeq 13.5$ mag corresponds to $R_c \simeq 16$ mag while the LCRS survey is over the range $R_c = 15$ to 18 mag). The minimal color differences are probably a symptom of the aperture biases affecting the LCRS spectral classifications, in which

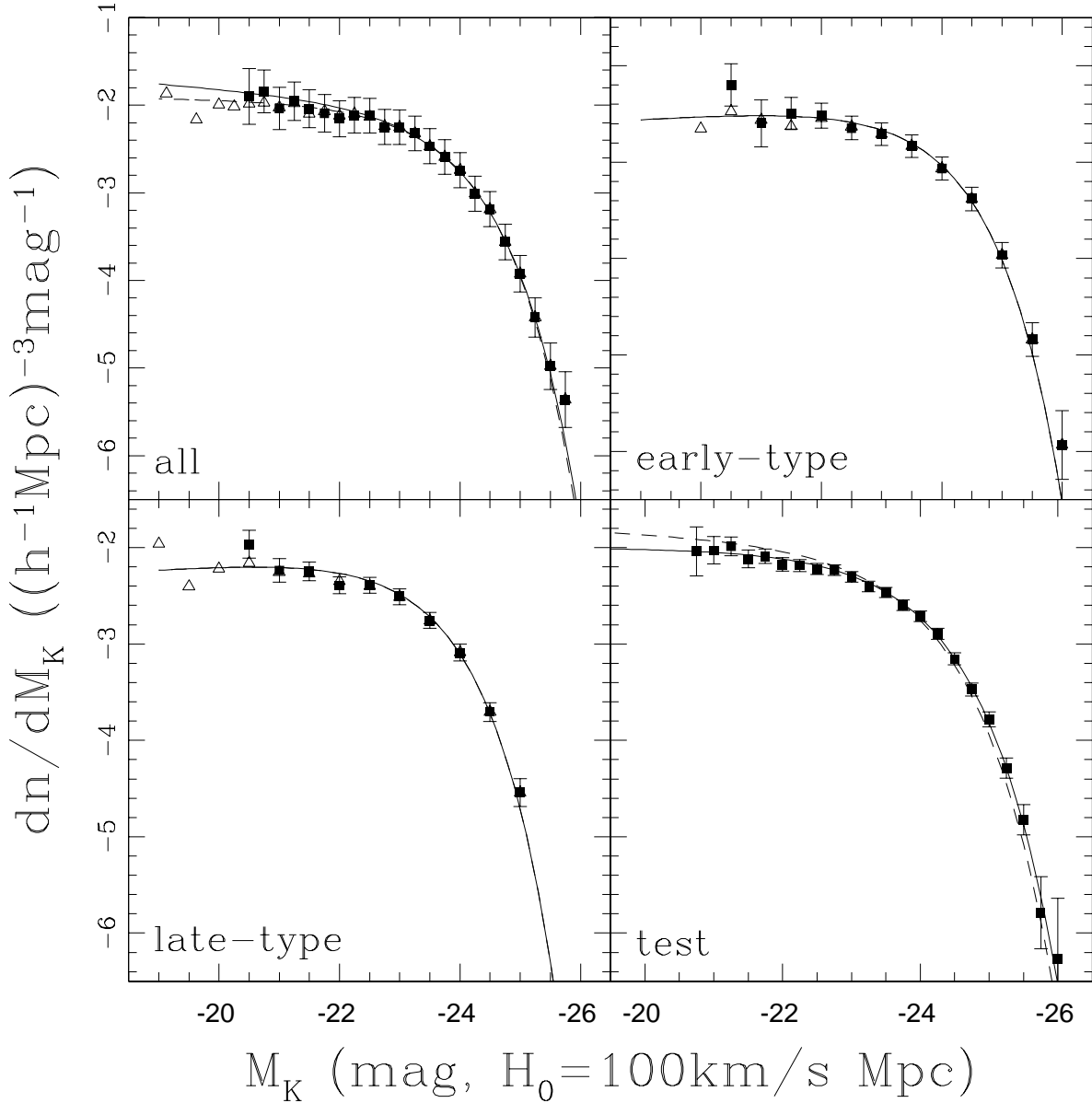


Fig. 3.— Luminosity function estimates. The four panels show the fit to the full sample (top left), the early-type galaxy sub-sample (top right), the late-type galaxy sub-sample (bottom left) and a Monte Carlo test (bottom right). The points are the non-parametric SWML model of the luminosity function and the curves are the best fit Schechter functions found with the STY method. The filled squares with error bars and the solid line are for the $cz > 2000 \text{ km s}^{-1}$ sample, while the open triangles without error bars and the dashed line are for the $cz > 1000 \text{ km s}^{-1}$ sample. For $M_K \lesssim -21 \text{ mag}$ the symbols for the two samples are superposed. The dashed curve in the Monte Carlo test panel is the input luminosity function, which was chosen to match the best fit to the full sample. The error bars are highly correlated and include the global uncertainty in the density normalization. Only bins containing at least four galaxies are shown.

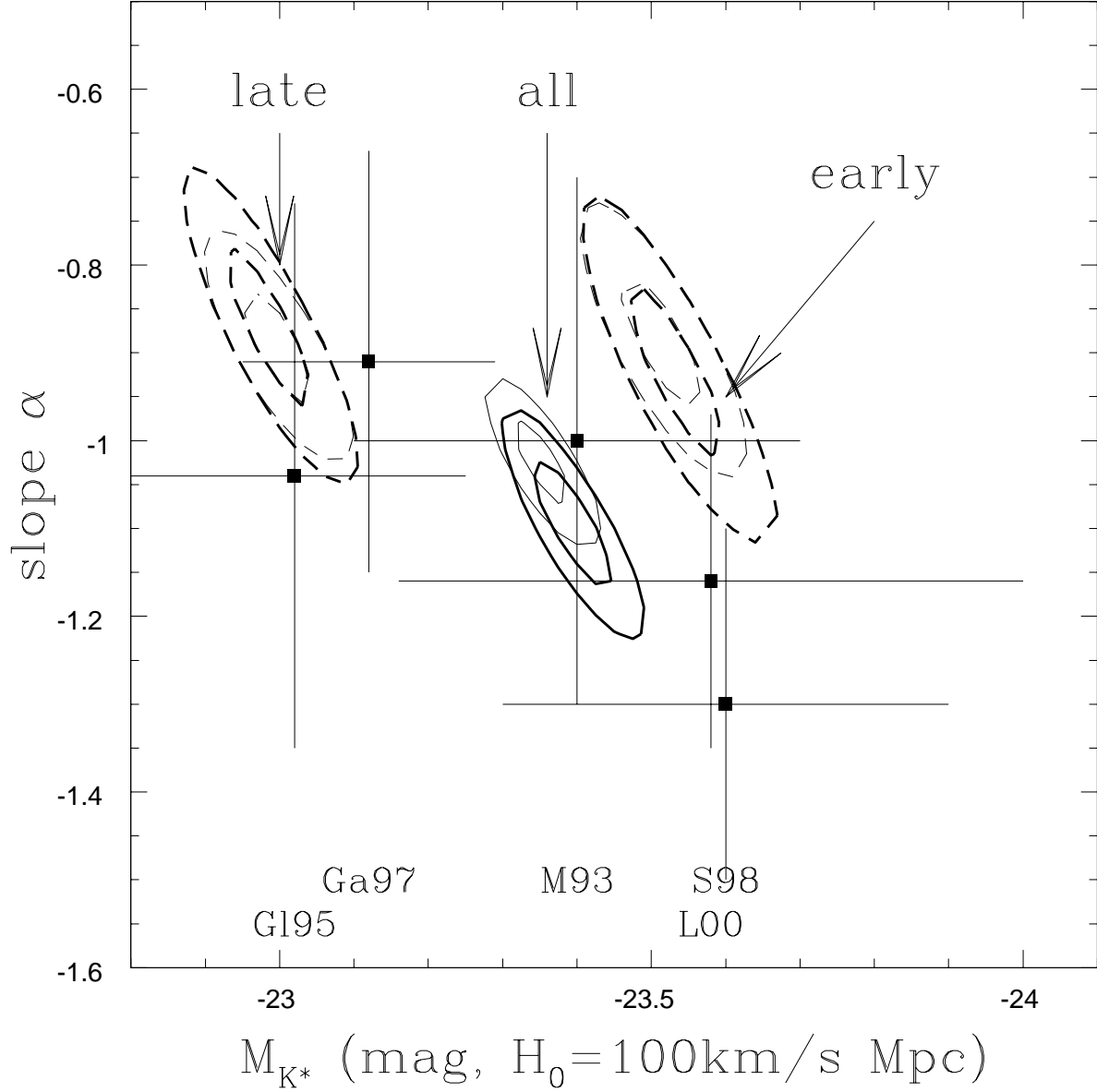


Fig. 4.— Schechter function parameter likelihoods. The 1σ and 2σ likelihood contours for one parameter are shown for the Schechter function parametric fits to the early-type galaxy sub-sample (left, dashed), the full sample (middle, solid) and the late-type galaxy sub-sample (right, dashed). The heavy contours are for the $cz > 2000 \text{ km s}^{-1}$ sample and the light contours are for the $cz > 1000 \text{ km s}^{-1}$ sample. The points with error bars show results from the literature as compiled and standardized by Loveday (2000). The points are (from left to right), Szokoly et al. (1998, S98), Loveday (2000, L00), Mobasher et al. (1993, M93), Glazebrook et al. (1995, G195), and Gardner et al. (1997, Ga97). The uncertainties from the present sample are significantly smaller because the sample is complete and approximately 10 times larger.

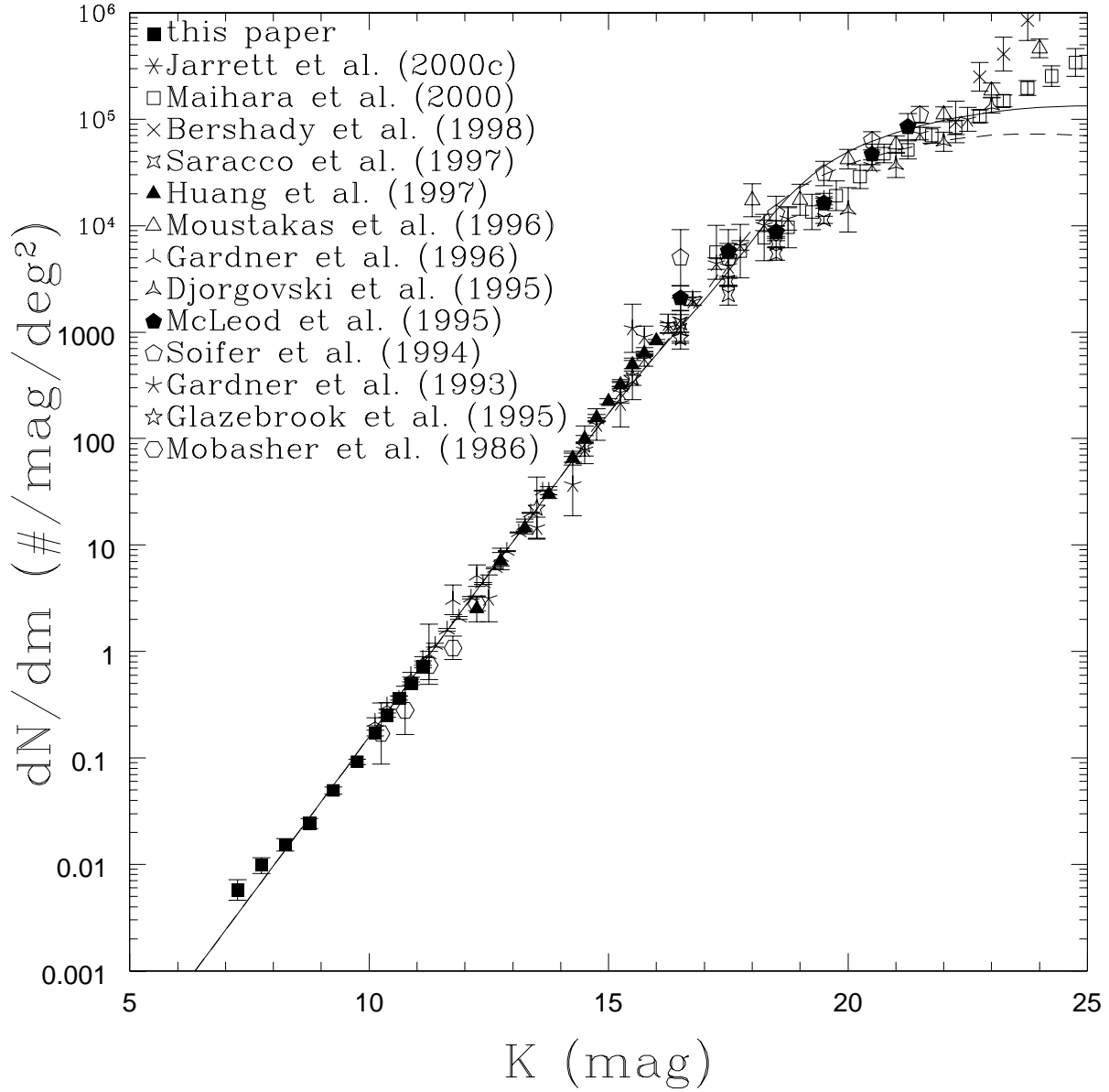


Fig. 5.— Differential K-band galaxy number counts. The points show the results of a wide range of surveys including the number counts of our sample. The solid (dashed) curve shows the predictions for a formation epoch of $z_f = 5$ ($z_f = 3$). Our local counts and luminosity functions use K_s -band isophotal magnitudes (see §2). We made no corrections for the differences between the K, K_s and K' filters and made no attempt to standardize the definitions of the galaxy magnitudes.

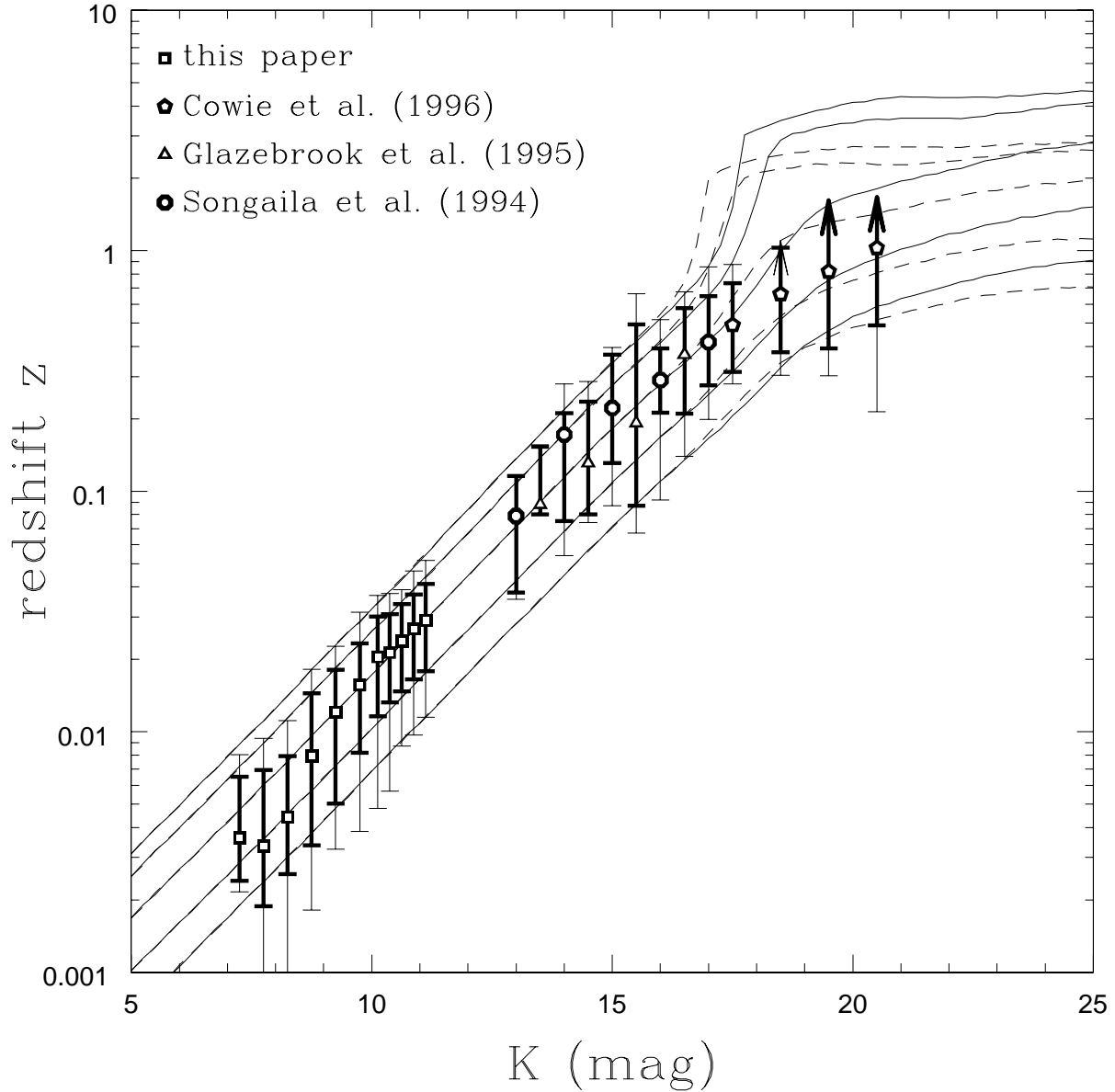


Fig. 6.— Redshift distributions predicted by pure luminosity evolution models. The solid (dashed) curves are contours of the redshift distribution for formation epochs of $z_f = 5$ ($z_f = 3$). From top to bottom, 95%, 84% (1σ above the median), 50% (the median), 16% (1σ below the median), and 5% of galaxies are predicted to have lower redshifts than the corresponding curve. The points and error bars show the distributions observed in our sample and the fainter samples of Songaila et al. (1994), Glazebrook et al. (1995) and Cowie et al. (1996). The points correspond to the sample median at each magnitude, the heavy error bars span the 1σ region (16% to 84% of the sorted sample), and the light error bars span the 5% to 95% region. To construct the sample statistics, unobserved objects were assumed to have the median redshift, and objects with unmeasured redshifts were assumed to lie at high redshift. An arrow indicates that the upper limit would be due to the objects with unmeasured, but assumed to be high, redshifts, with the tip of the arrow located at the highest measured redshift.

bright late-type galaxies are misclassified as early-type galaxies (see Kochanek et al. 2000). The mismatch of the color differences between types and the color dispersion for the individual types becomes larger when the sample is divided more finely using the spectral clan classification of the LCRS galaxies by Bromley et al. (1998).

The colors do not provide a simple explanation for the M_* differences between the various surveys. For example, $\langle B - K \rangle \simeq 3.45 \pm 0.07$ mag for the APM (B_J mags), CfA (B_Z Zwicky mags) and SSRS2 ($B(0)$ mags) surveys even though the characteristic magnitude of the CfA survey is 0.7 mag fainter than the APM and SSRS2 surveys. The colors of the early-type galaxies in the CfA and SSRS2 surveys are very similar, while their colors in the APM survey are 0.3 mag bluer. This is consistent with the incompleteness in the APM morphological classifications being dominated by the more distant, red early-type galaxies (see Loveday et al. 1992, Marzke et al. 1994b). With the exception of the Sa/Sb galaxies in the CfA survey, which are relatively red and have an anomalous value for α , the late-type galaxies in the three surveys have very similar colors.

5. Comparisons to the Properties of Faint Infrared Samples

One important use of local luminosity functions is in estimates of the properties of fainter or higher redshift galaxies. Here we make some comparisons to the magnitude and redshift distributions of fainter infrared galaxies using simple evolution models. We combined our luminosity functions with Bruzual & Charlot (1993, GISEL96 version) galaxy evolution models assuming an $\Omega_0 = 0.3$ flat cosmological model and $H_0 = 65 \text{ km s}^{-1} \text{ Mpc}^{-1}$ to determine the distances and ages. We considered no evolution models (K-corrections only) and evolving models using an “Sb” template for the late-type galaxies (based the star formation history models of Guiderdoni & Rocca-Volmerange 1988) and an 1 Gyr exponential burst ($SFR \propto \exp(-(t - t_f)/\text{Gyr})$) for the early-type galaxies where the populations formed at $z_f = 3$ or 5. We predicted the number counts and redshift distributions of galaxies as a function of magnitude, and compared them to the available observational data. All the models are consistent with the number counts and redshift distributions measured for our low redshift sample (see Figs. 5 and 6), confirming that we have derived luminosity functions consistent with our data. Table 6 presents the number counts for our current sample.

It is no surprise that no evolution models with a finite formation epoch are unable to reproduce either the number counts or the redshift distributions. The predicted counts lie below the observations and the predicted redshifts are systematically lower than observed once $K \gtrsim 16$ mag. Particularly for early-type galaxies, there is direct evidence that the infrared luminosities evolve significantly by redshift unity. Pahre (2000) used the fundamental plane to measure the amount of surface brightness evolution of cluster early-type galaxies to $z \simeq 0.5$, de Propris et al. (2000) measured the evolution of the cluster luminosity functions to $z \simeq 1$, and Kochanek et al. (2000) used the fundamental plane of gravitational lenses to measure the surface brightness evolution of field early-type galaxies to $z \simeq 1$. All three estimates require stellar populations formed in short bursts at $z_f = 2-5$ rather than no evolution models.

Pure luminosity evolution models, where the comoving numbers of galaxies are fixed but the stellar populations are allowed to evolve, work far better. Figures 5 and 6 show that populations

formed at $z_f = 3$ or 5 are relatively consistent with both the number counts and the redshift distributions for $K \lesssim 18$ mag. At fainter magnitudes these models begin to have too low a surface density and too high an average redshift. The high redshift tail in the distribution is due to the $z \gtrsim 1$ early-type galaxies, which are predicted to be very luminous. Kauffmann & Charlot (1998) use this disagreement and their semi-analytic models of galaxy formation to argue that many L_* early-type galaxies must be formed from mergers occurring near redshift unity. Indeed, crude merger models with $n_* \propto (1+z)^\gamma$, $L_* \propto 1/n_*$ to conserve the total mass and $\gamma \simeq 1$ naturally eliminate the high redshift tail and increase the number counts of faint galaxies.

Unfortunately, many of the differences could be created by sample variance rather than rapid merging. We can see the effects of sample variance in Fig. 6 both at $z \lesssim 0.01$ for our sample and in the differences between the redshift distributions found by Glazebrook et al. (1995) and Songaila et al. (1994) at similar apparent magnitudes. While the differences in the survey geometries (equal axes versus pencil beam) mean that large scale structure affects the survey statistics differently, our comoving volume out to $z = 0.01$ is 30 times larger than the survey volume of the Cowie et al. (1996) fields out to redshift unity. If we link galaxies in the Cowie et al. (1996) fields with velocity differences smaller than 1000 km s^{-1} into single “objects” (to try to suppress the effects of correlated structures on the redshift distribution), the median redshift increases significantly (by $\Delta z \simeq 0.2$). Thus, significantly larger redshift samples are needed to quantitatively test evolutionary models.

6. Summary

We have derived the first local infrared galaxy sample whose statistical uncertainties are comparable to those of local optical galaxy luminosity functions. We derived both total and morphologically-typed luminosity functions. Our morphological types are self-consistent (see Kochanek et al. 2000) and our luminosity functions are insensitive to random errors in the classifications and the parameters change as expected when we shift the boundary between early and late-type galaxies. Like morphologically-typed optical surveys (CfA and SSRS2), we find that the luminosity functions of early and late-type galaxies have similar shapes, $\alpha \simeq -0.9 \pm 0.1$, in marked contrast to spectrally-typed optical surveys (ESO Slice, LCRS, 2dFGRS) which usually find that the slope steepens for late-type galaxies. Note, however, that in Kochanek et al. (2000) we find that the spectral classification methods are not self-consistent because of the aperture bias created by using a spectroscopic aperture that is much smaller than the galaxies being observed. We used galaxies found in both the optical redshift surveys and the 2MASS survey to estimate the magnitude differences between 2MASS and the optical surveys and also between the different optical surveys. In all surveys, later type galaxies have bluer optical to infrared colors, but the magnitude differences cannot fully explain the discrepancies between the magnitude scales of the luminosity functions. Our luminosity functions successfully predict the properties of fainter infrared samples until $K \gtrsim 18$ mag where the models have a significant dependence on galaxy evolution and merging histories and the comparison data is probably affected by sample variance.

These results are preliminary, and the sample is still growing rapidly. In particular, the survey area complete to the current magnitude limit continues to expand rapidly, and it is easy to

build complete, deeper samples in restricted areas to extend to fainter absolute magnitude limits. With complete sky coverage we can use the 2MASS catalog to probe the relative completeness of redshift surveys and to improve our comparisons between the survey magnitude scales. By combining this with the surface photometry available for 2MASS galaxies we can quantitatively explore the effects of surface brightness selection effects (e.g. Disney 1976, Sprayberry et al. 1997, Dalcanton et al. 1997, Huchra 1999, Cross et al. 2000) on large redshift surveys. As the coverage gaps are eliminated we can look at density dependences to galaxy properties. In Pahre et al. (2000) we derive an improved galaxy velocity function ($dn/d\log v$ instead of dn/dM) based on the Tully-Fisher and Faber-Jackson relations derived from the same 2MASS photometry used to derive the luminosity function. The velocity function is useful because it determines the optical depth of the universe to gravitational lensing (see Falco, Kochanek & Munoz 1998) and can be used to probe the evolution of galaxies (see Gonzalez et al. 2000).

Acknowledgements: This research was supported by the Smithsonian Institution. The authors thank P. Berlind and M. Calkins, the FLWO remote observers, for obtaining the redshift data, and S. Tokarz for the data reduction. We thank J. Loveday for his compilation of infrared luminosity function estimates. M.A.P. was supported by Hubble Fellowship grant HF-01099.01-97A from STScI (which is operated by AURA under NASA contract NAS5-26555).

REFERENCES

- Andreon, S., & Pello, R., 2000, *A&A*, 353, 479
- Bershady, M.A., Lowenthal, J.D., & Koo, D.C., 1998, *ApJ*, 505, 50
- Bromley, B.C., Press, W.H., Lin, H., & Kirshner, R.P., 1998, *ApJ*, 505, 25
- Bruzual, A.G., & Charlot, S., 1993, *ApJ*, 405, 538
- Cardelli, J.A., Clayton, G.C., & Mathis, J.S., 1989, *ApJ*, 345, 245
- Cowie, L.L., Gardner, J.P., Hu, E.M., Songaila, A., Hodapp, K.-W., & Wainscoat, R.J., 1994, *ApJ*, 434, 114
- Cowie, L. L., Songaila, A., Hu, E. M., & Cohen, J. G. 1996, *AJ*, 112, 839
- Cross, N., Driver, S., & Lemon, D., 2000, in “The New Era of Wide-Field Astronomy”, eds. R.G. Clowes, A.J. Adamson, & G.E. Bromage (San Francisco: ASP) astro-ph/0010418
- da Costa, L.N., Willmer, C.N.A., Pellegrini, P.S., Chaves, O.L., Rite, C., Maia, M.A.G., Geller, M.J., et al., 1998, *AJ*, 116, 1
- da Costa, L.N., Geller, M.J., Pellegrini, P.S., Latham, D.W., Fairall, A.P., Marzke, R.O., Willmer, C.N.A., Huchra, J.P., Calderon, J.H., Ramella, M., & Kurtz, M.J., 1994, *ApJ*, 424, 1
- Dalcanton, J.J., Spergel, D.N., Gunn, J.E., Schmidt, M., & Schneider, D.P., 1997, *AJ*, 114, 635

- Davis, M., & Huchra, J., 1982, *ApJ*, 254, 437
- de Lapparent, V., Geller, M.J., & Huchra, J.P., 1988, *ApJ*, 332, 44
- de Propris, R.D., Eisenhardt, P.R., Stanford, S.A., & Dickinson, M., 1998, *ApJL*, 503, L45
- de Propris, R.D., Stanford, S.A., Eisenhardt, P.R., Dickinson, M., & Elston, R., 1999, *AJ*, 118, 719
- de Vaucouleurs, G., de Vaucouleurs, A., & Crowin, H.G., 1976, *Second Reference Catalogue of Bright Galaxies* (Univ. of Texas Press: Austin)
- Disney, M., 1976, *Nature*, 263, 573
- Djorgovski, S., Soifer, B.T., Pahre, M.A., Larkin, J.E., Smith, J.D., Neugebauer, G., Smail, I., Matthews, K., Hogg, D.W., Blandford, R.D., Cohen, J., Harrison, W., & Nelson, J., 1995, *ApJL*, 438, 13
- Dressler, A. 1980, *ApJ*, 236 351
- Efstathiou, G., Ellis, G., & Peterson, B.A., 1988, *MNRAS*, 232, 431
- Fabricant, D., Cheimets, P., Caldwell, N. & Geary, J., 1998, *PASP*, 110, 79
- Falco, E.E., Kochanek, C.S., & Munoz, J.A., 1998, *ApJ*, 494, 47
- Falco, E.E., Kurtz, M.J., Geller, M.J., Huchra, J.P., Peters, J., Berlind, P., Mink, D.J., Tokarz, S.P., & Elwell, B., 1999, *PASP*, 111, 438
- Folkes, S., Ronen, S., Price, I., Lahav, O., Colless, M., Maddox, S., et al., 1999, *MNRAS*, 308, 459
- Gardner, J.P., Cowie, L.L., & Wainscoat, R.J., 1993, *ApJ*, 415, 9
- Gardner, J.P., Sharples, R.M., Carrasco, B.E., & Frenk, C.S., 1996, *MNRAS*, 282, 1
- Gardner, J.P., Sharples, R.M., Frenk, C.S., & Carrasco, B.E., 1997, *ApJL*, 480, L99
- Gavazzi, G., Pierini, D., & Boselli, A., 1996, *A&A*, 312, 397
- Geller, M., & Huchra, J.P., 1989, *Science*, 246, 897
- Geller, M., Kurtz, M.J., Wegner, G., Thorstensen, J.R., Fabricant, D.G., Marzke, R.O., Huchra, J.P., Schild, R.E., & Falco, E.E., 1997, *AJ*, 114, 2205
- Glazebrook, K., Peacock, J.A., Collins, C.A., & Miller, L. 1994, *MNRAS*, 266, 65
- Glazebrook, K., Peacock, J.A., Miller, L., & Collins, C.A., 1995, *MNRAS*, 275, 169
- Gonzalez, A.H., Williams, K.A., Bullock, J.S., Kolatt, T.S. & Primack, J.R., 2000, *ApJ*, 528, 145
- Guiderdoni, B., & Rocca-Volmerange, B., 1988, *A&AS*, 74, 185

- Huang, J.-S., Cowie, L.L., Gardner, J.P., Hu, E.M., Songaila, A., & Wainscoat, R.J., 1997, *ApJ*, 476, 12
- Huchra, J., 1999, in *The Low Surface Brightness Universe*, IAU 171, J. I. Davies, C. Impey & S. Phillips, eds., (San Francisco: ASP) 45
- Huchra, J.P., Geller, M.J., Clemens, C.M., Tokarz, S.P., & Michel, A., 1992, *Bull. CDS*, 41, 31 (Strasbourg)
- Jarrett, T.-H., Chester, T., Cutri, R., Schneider, S., Rosenberg, J., Huchra, J.P., & Mader, J., 2000a, *AJ*, 120, 298
- Jarrett, T., et al., 2000b, in preparation
- Jarrett, T., Chester, T., Cutri, R., Schneider, S., Skrutskie, M., & Huchra, J.P., 2000c, in preparation
- Kauffmann, G., & Charlot, S., 1998, *MNRAS*, 297, L23
- Kochanek, C.S., Falco, E.E., Impey, C.D., Lehar, J., McLeod, B.A., Rix, H.-W., Keeton, C.R., Munoz, J.A., & Peng, C.Y., 2000, *ApJ*, 543, 131
- Kochanek, C.S., Pahre, M.A., & Falco, E.E., 2000, in preparation
- Kurtz, M.J., & Mink, D.J., 1998, *PASP*, 110, 934
- Lilly, S. J., Tresse, L., Hammer, F., Crampton, D., & Le Fèvre, O. 1995, *ApJ*, 455, 108
- Lin, H., Kirshner, R.P., Shectman, S.A., Landy, S.D., Oemler, A., Tucker, D.L., & Schechter, P.L., 1996, *ApJ*, 464, 60
- Loveday, J., Peterson, B.A., Efstathiou, G., & Maddox, S.J., 1992, *ApJ*, 390, 338
- Loveday, J., Peterson, B.A., Efstathiou, G., & Maddox, S.J., 1996, *ApJS*, 107, 201
- Loveday, J., 2000, *MNRAS*, 312, 557
- Maihara, T., Iwamuro, F., Tanabe, H., Taguchi, T., Hata, R., Oya, S., Kashikawa, N., et al., 2000, *PASJ*, in press (astro-ph/0009409)
- Marzke, R.O., Huchra, J.P., & Geller, M.J., 1994a, *ApJ*, 428, 43
- Marzke, R.O., Geller, M.J., Huchra, J.P., & Corwin, H.G., 1994b, *AJ*, 108, 437
- Marzke, R.O., da Costa, L.N., Pellegrini, P.S., Willmer, C.N.A., & Geller, M.J., 1998, *ApJ*, 503, 617
- McLeod, B.A., Bernstein, G.M., Rieke, M.J., Tollestrup, E.V., & Fazio, G.G., 1995, *ApJS*, 96, 117
- Mobasher, B., Sharples, R.M., & Ellis, R.S., 1986, *MNRAS*, 223, 11
- Mobasher, B., Sharples, R.M., & Ellis, R.S., 1993, *MNRAS*, 263, 560

- Moustakas, L.A., Davis, M., Grahan, J.R., Silk, J., Peterson, B.A., & Yoshii, Y., 1997, *ApJ*, 475, 445
- Naim, A., Lahav, O., Sodre, L., & Storrie-Lombardi, M.C., 1995a, *MNRAS*, 275, 567
- Naim, A., Lahav, O., Buta, R.J., Corwin, H.G., de Vaucouleurs, G., Dressler, A., Huchra, J.P., van den Bergh, S., Raychaudhury, S., Sodre, L., & Storrie-Lombardi, M.C., 1995b, *MNRAS*, 274, 1107
- Pahre, M.A., 1999, *ApJ* submitted
- Pahre, M.A., Kochanek, C.S., & Falco, E.E., 2000, in preparation
- Saracco, P., Iovino, A., Garilli, B., Maccagni, D., & Chincarini, G., 1997, *AJ*, 114, 887
- Sandage, A., Tammann, G.A., & Yahil, A., 1979, *ApJ*, 232, 352
- Schechter, P., 1976, *ApJ*, 203, 297
- Schlegel, D.J., Finkbeiner, D.P., & Davis, M., 1998, *ApJS*, 500, 525
- Shectman, S.A., Landy, S.D., Oemler, A., Tucker, D.L., Lin, H., Kirshner, R.P., & Schechter, P.L., 1996, *ApJ*, 470, 172
- Skrutskie, M.F., Schneider, S.E., Stiening, R., Strom, S.E., Weinberg, M.D., Beichman, C., Chester, T., et al., 1997, in *The Impact of Large Scale Near-IR Sky Surveys*, F. Garzon et al., eds., (Dordrecht: Kluwer) 187
- Slonim, N., Somerville, R., Tishby, N., & Lahav, O., 2000, submitted to *MNRAS*, astro-ph/0005306
- Soifer, B.T., Matthews, K., Djorgovski, S., Larkin, J., Graham, J.R., Harrison, W., Jernigan, G., Lin, S., Nelson, J., Neugebauer, G., Smith, G., Smith, J.D., & Ziomkowski, C., 1994, *ApJL*, 420, 1
- Songaila A., Cowie L.L., Hu E.M., & Gardner J.P., 1994, *ApJS*, 94, 461
- Sprayberry, D., Impey, C.D., Irwin, M.J., & Bothun, G.D., 1997, *ApJ*, 482, 104
- Szokoly, G.P., Subbarao, M.U., Connolly, A.J., & Mobasher, B., 1998, *ApJ*, 492, 452
- Tonry, J.L., Blakeslee, J.P., Ajhar, E.A., & Dressler, A., 2000, *ApJ*, 530, 625
- Vettolani, G., Zucca, E., Zamorani, G., et al., 1997, 325, 954
- Worthey, G., 1994, *ApJS*, 95, 107
- York, D.G., Adelman, J., Anderson, J.E., et al., 2000, astro-ph/0006396
- Zucca, E., Zamorini, G., Vettolani, G., Cappi, A., Merighi, R., Mignoli, M., Stirpe, G.M., et al., 1997, *A&A*, 326, 477

Table 1. The Galaxy Sample

Target	cz km s ⁻¹	ref. code	K_{20} mag	T-type	Bar	Pec?	Int?
2MJ000009.1+324418	10372	2779	10.59	-4.2 ± 1.3			
2MJ000028.8+324656	9803	2700	10.89	-4.9 ± 0.1			Y
2MJ000038.0+282305	8705	2212	10.52	1.5 ± 0.9			
2MJ000044.0+282405	8157	2779	11.22	2.3 ± 1.0	B		Y
2MJ000047.0+282407	8764	2779	10.33	-4.0 ± 1.5			Y
2MJ000058.9+285442	6899	2212	11.09	2.0 ± 1.0	X		
2MJ000103.6+343911	12684	-160	11.16	2.0 ± 1.0			
2MJ000114.1+344032	12953	2779	11.08	3.0 ± 1.0	BX		Y
2MJ000119.7+343132	5032	5502	10.62	2.5 ± 1.0			
2MJ000126.7+312600	4948	2700	10.26	-3.5 ± 1.5	X	Y	Y
2MJ000130.0+312630	4767	2212	10.42	3.7 ± 1.0		Y	Y
2MJ000138.3+232902	4371	0620	9.27	5.1 ± 0.1			Y
2MJ000141.9+232944	4336	0620	9.94	4.6 ± 0.9		Y	Y
2MJ000246.0+185311	7882	0650	10.86	1.7 ± 1.0	X		
2MJ000309.6+215736	6600	2212	10.49	2.5 ± 0.9		Y	
2MJ000329.2+272106	7690	2700	11.06	0.1 ± 1.5	X		
2MJ000335.0+231202	7254	0668	10.97	4.4 ± 1.0	X		
2MJ000358.7+204502	2310	0658	8.57	4.6 ± 0.9			
2MJ000433.7+281805	8785	2700	10.61	-3.0 ± 1.5			
2MJ000548.3+272657	7531	0624	10.92	3.0 ± 1.0	B		
2MJ000640.1+260916	7552	2700	11.12	2.0 ± 1.6			
2MJ000842.4+372652	4389	0649	10.05	-0.3 ± 1.4			
2MJ000932.7+331831	4901	2700	9.49	-3.8 ± 1.5			
2MJ001040.8+325858	4788	0668	10.64	3.8 ± 1.0	B		
2MJ001046.8+332110	4765	0668	10.49	3.6 ± 1.0	X		
2MJ001101.0+300307	6791	2212	10.18	2.3 ± 1.0	X		
2MJ001143.1+205832	13900	0300	10.99	-3.6 ± 1.8			
2MJ001151.3+330623	14058	2700	11.19	-3.6 ± 1.8			
2MJ001215.7+221918	7629	0624	10.69	1.0 ± 0.9			
2MJ001218.8+310339	4857	2212	10.87	4.8 ± 0.7			

Note. — The first 30 entries of the catalog. The redshift cz is the measured heliocentric velocity and K_{20} is the isophotal apparent magnitude (see Jarrett et al. 2000a). The ZCAT format reference code for the source of the redshift measurement is given by the “ref. code” entry (see <http://cfa-www.harvard.edu/~huchra/zcat/zsource.tex>). The error bar on the T-type classification is the standard error based on the scatter in the two or more classifications for the object. In the Bar column we flag objects which at least one classifier flagged as having a full (B) or incipient bar (X). In the Pec? and Int? columns we flag objects which were considered to be peculiar or interacting by at least one classifier.

Table 2. 2MASS Non-Parametric Luminosity Functions

M_K (mag)	all			early-type			late-type		
	N	$\log(n)$	σ	N	$\log(n)$	σ	N	$\log(n)$	σ
-26.00	1	-6.34	0.66	4	-5.93	0.36			
-25.75	9	-5.36	0.32						
-25.50	16	-4.98	0.27	37	-4.84	0.17	3	-5.81	0.45
-25.25	41	-4.42	0.23						
-25.00	94	-3.92	0.21	160	-3.97	0.13	33	-4.54	0.15
-24.75	169	-3.56	0.20						
-24.50	308	-3.19	0.20	389	-3.38	0.12	173	-3.71	0.10
-24.25	356	-3.01	0.20						
-24.00	494	-2.74	0.20	457	-3.06	0.12	471	-3.09	0.09
-23.75	494	-2.59	0.20						
-23.50	437	-2.47	0.20	359	-2.83	0.12	529	-2.76	0.08
-23.25	401	-2.32	0.20						
-23.00	327	-2.25	0.20	210	-2.71	0.12	428	-2.51	0.08
-22.75	206	-2.25	0.20						
-22.50	191	-2.12	0.20	94	-2.65	0.12	261	-2.39	0.08
-22.25	127	-2.11	0.20						
-22.00	65	-2.15	0.21	43	-2.52	0.13	106	-2.39	0.09
-21.75	43	-2.09	0.21						
-21.50	33	-2.04	0.22	16	-2.49	0.16	56	-2.25	0.10
-21.25	28	-1.95	0.22						
-21.00	15	-2.04	0.24	6	-2.60	0.24	26	-2.24	0.12
-20.75	14	-1.84	0.24						
-20.50	5	-1.90	0.32	5	-2.20	0.22	11	-1.96	0.15
-20.25	3	-1.00	0.21						

Note. — The SWML binned luminosity functions as a function of absolute magnitude M_K where $\log(n)$ is the logarithm of the comoving density (number/ $h^{-3}\text{Mpc}^3 \text{ mag}$) and σ is its uncertainty. The late-type and early-type luminosity functions were derived using $\Delta M = 0.5 \text{ mag}$ bins widths, twice that for the full sample. The errors for the individual bins are very highly correlated and cannot be used directly if the uncertainty weightings are quantitatively important.

Table 3. 2MASS Parametric Luminosity Functions

Name	Type	N	K_* mag	α	n_* $10^{-2}h^3 \text{ Mpc}^{-3}$
Standard	all	3878	-23.39 ± 0.05	-1.09 ± 0.06	1.16 ± 0.10
	late	2097	-22.98 ± 0.06	-0.87 ± 0.09	1.01 ± 0.13
$cz > 1000 \text{ km s}^{-1}$	early	1781	-23.53 ± 0.06	-0.92 ± 0.10	0.45 ± 0.06
	all	4096	-23.35 ± 0.04	-1.02 ± 0.05	1.19 ± 0.10
	late	2244	-23.00 ± 0.05	-0.89 ± 0.07	1.00 ± 0.12
Bootstrap	early	1852	-23.51 ± 0.06	-0.89 ± 0.08	0.46 ± 0.06
	late	–	-23.02 ± 0.06	-0.96 ± 0.09	0.91 ± 0.10
Boundary $T = -1.5$	early	–	-23.52 ± 0.05	-0.90 ± 0.09	0.48 ± 0.04
	late	2311	-22.98 ± 0.06	-0.87 ± 0.09	1.14 ± 0.14
Boundary $T = 0.5$	early	1567	-23.55 ± 0.07	-0.85 ± 0.11	0.38 ± 0.05
	late	1827	-22.98 ± 0.06	-0.87 ± 0.10	0.88 ± 0.13
Boundary $T = 1.5$	early	2051	-23.52 ± 0.06	-0.99 ± 0.09	0.53 ± 0.06
	late	1472	-23.02 ± 0.07	-0.94 ± 0.10	0.68 ± 0.10
	early	2406	-23.47 ± 0.06	-0.99 ± 0.08	0.66 ± 0.07

Note. — The standard model uses a velocity limit $cz > 2000 \text{ km s}^{-1}$ and the boundary between early-type and late-type galaxies is $T = -0.5$. The Name column shows the change made to the standard model to derive that case’s parameters. The Bootstrap case randomly resamples the galaxies with replacement, including Poisson variations in the number of galaxies and the addition of random errors to the morphological types (see text). Its density uncertainties do not include the contribution from sample variance due to large scale structure. We present the Schechter function parameters K_* , α and n_* (eqn. 2), and we used $H_0 = 100h \text{ km s}^{-1} \text{ Mpc}^{-1}$ in estimating K_* and n_* .

Table 4. Previous Infrared Luminosity Functions

Sample	N	K_* mag	α	n_* $10^{-2}h^3 \text{ Mpc}^{-3}$	Type
Mobasher et al. 1993	181	-23.4 ± 0.3	-1.0 ± 0.3	1.12 ± 0.16	optically selected
Glazebrook et al. 1995	335	-23.02 ± 0.23	-1.04 ± 0.31	2.90 ± 0.70	redshift, 37% complete
Gardner et al. 1997	567	-23.12 ± 0.17	-0.91 ± 0.24	1.66	redshift, 90% complete
Szokoly et al. 1998	867	-23.6 ± 0.3	-1.3 ± 0.2	1.2 ± 0.4	redshift, 31% complete
Loveday 2000	345	-23.58 ± 0.42	-1.16 ± 0.19	1.2 ± 0.8	optically selected
de Propris et al. 2000		-23.3 ± 0.7	-0.8 ± 0.4	–	Coma cluster

Note. — Table derived from Loveday (2000). The *optically selected* surveys used K-band imaging of galaxies from a complete but optically selected redshift survey, and the *redshift* surveys obtained redshifts for objects selected from an infrared imaging survey. De Propris et al. (2000) constructed a volume limited sample in the Coma cluster. Mobasher et al. (1993) magnitudes have been adjusted by 0.22 mag due to K-correction differences (see Glazebrook et al. 1995; Gardner et al. 1997). An aperture correction of -0.30 is added to the Glazebrook et al. (1995) magnitudes (see Gardner et al. 1997). We show the Glazebrook et al. (1995) results for $z < 0.2$, which includes only 55 galaxies with redshifts. Gardner et al. (1997) contains no estimate for the uncertainties in n_* . The Poisson uncertainties are $0.07 \times 10^{-2}h^3 \text{ Mpc}^{-3}$, but the true error will be dominated by sample variance due to the finite survey volume. All the results are scaled to $H_0 = 100h \text{ km s}^{-1} \text{ Mpc}^{-1}$.

Table 5. Optical Luminosity Functions

Survey	type	N	band	M_* mag	$\langle m - K_{20} \rangle$ mag	α	n_* $10^{-2} h^3 \text{ Mpc}^{-3}$	Ref
APM	all	1658	B_J	-19.50 ± 0.13	3.39 ± 0.62	-0.97 ± 0.15	1.40 ± 0.17	1
	early	311		-19.71 ± 0.25	3.73 ± 0.47	0.20 ± 0.35		1
	late	999		-19.40 ± 0.16	3.25 ± 0.68	-0.80 ± 0.20		1
Century	all	1762	R_c	-20.73 ± 0.18	4.10 ± 0.65	-1.17 ± 0.19	2.50 ± 0.60	2
CfA	all	9063	B_Z	-18.80 ± 0.30	3.46 ± 0.89	-1.00 ± 0.20	4.00 ± 1.00	3
	E			-19.23 ± 0.2	4.10 ± 0.65	-0.85 ± 0.20	0.15 ± 0.04	4
	S0			-18.74 ± 0.1	3.95 ± 0.65	-0.94 ± 0.15	0.76 ± 0.20	4
	Sa/b			-18.72 ± 0.1	3.79 ± 0.56	-0.58 ± 0.15	0.87 ± 0.22	4
	Sc/d			-18.81 ± 0.2	3.34 ± 0.64	-0.96 ± 0.15	0.44 ± 0.11	4
	Sm/Im			-18.79 ± 0.5	2.40 ± 0.73	-1.87 ± 0.20	0.06 ± 0.02	4
ESP	all	3342	B_J	-19.61 ± 0.08		-1.22 ± 0.07	2.00 ± 0.4	5
	em	1575		-19.47 ± 0.10		-1.40 ± 0.10	1.00 ± 0.2	5
	not-em	1767		-19.62 ± 0.10		-0.98 ± 0.09	1.10 ± 0.2	5
LCRS	all	18678	R_c	-20.29 ± 0.02	2.43 ± 0.28	-0.70 ± 0.03	1.90 ± 0.1	6
	not-em	11366		-20.22 ± 0.02	2.48 ± 0.21	-0.27 ± 0.04	1.10 ± 0.1	6
	em	7312		-20.03 ± 0.03	2.32 ± 0.35	-0.90 ± 0.04	1.30 ± 0.1	6
	1	655		-20.28 ± 0.07	2.54 ± 0.17	0.54 ± 0.14	0.034 ± 0.003	7
	2	7614		-20.23 ± 0.03	2.50 ± 0.18	-0.12 ± 0.05	0.71 ± 0.06	7
	3	4667		-19.90 ± 0.04	2.44 ± 0.26	-0.32 ± 0.07	0.99 ± 0.13	7
	4	3210		-19.85 ± 0.05	2.33 ± 0.32	-0.64 ± 0.08	1.15 ± 0.21	7
	5	1443		-20.03 ± 0.09	2.18 ± 0.34	-1.33 ± 0.09	0.84 ± 0.22	7
	6	689		-20.01 ± 0.14	1.89 ± 0.38	-1.84 ± 0.11	1.31 ± 0.78	7
	SSRS2	all		5036	$B(0)$	-19.43 ± 0.06	3.55 ± 0.83	-1.12 ± 0.05
E/S0	1587	-19.37 ± 0.11	4.07 ± 0.58	-1.00 ± 0.09		0.44 ± 0.08	8	
Spiral	3227	-19.43 ± 0.08	3.32 ± 0.81	-1.11 ± 0.07		0.80 ± 0.14	8	
2dFGRS	Irr/pec	204	B_J	-19.78 ± 0.45	3.22 ± 1.04	-1.81 ± 0.24	0.20 ± 0.08	8
	all	5869		-19.73 ± 0.06		-1.28 ± 0.05	1.69 ± 0.17	9
	1	1850		-19.61 ± 0.09		-0.74 ± 0.11	0.90 ± 0.09	9
	2	928		-19.68 ± 0.14		-0.86 ± 0.15	0.39 ± 0.06	9
	3	1200		-19.38 ± 0.12		-0.99 ± 0.13	0.53 ± 0.08	9
	4	1193		-19.00 ± 0.12		-1.21 ± 0.12	0.65 ± 0.13	9
	5	668	-19.02 ± 0.22		-1.73 ± 0.16	0.21 ± 0.11	9	

Note. — For the color difference $\langle m - K_{20} \rangle$ we give the mean color and the dispersion in the color. The statistical uncertainty in the mean color is generally less than 0.05 mag and the mean color was calculated over a magnitude range such that the survey magnitude limits would not affect the colors. We cannot calculate $\langle m - K_{20} \rangle$ for the ESP (too little overlap with the current 2MASS catalog), Century (no published object lists), and 2dFGRS (no published object lists) surveys. References: (1) Loveday et al. (1992); (2) Geller et al. 1997; (3) Marzke et al. 1994a; (4) Marzke et al. 1994b; (5) Zucca et al. (1997); (6) Lin et al. 1996; (7) Bromley et al. 1998; (8) Marzke et al. 1998; (9) Folkes et al. 1999.

Table 6. Differential K_s -band Number Counts

K_s (mag)	ΔK_s (mag)	N	$\log(dN/dm)$ #/mag/deg ²	Poisson Errors
7.250	0.50	20	-2.24	0.097
7.750	0.50	36	-2.01	0.074
8.250	0.50	53	-1.82	0.060
8.750	0.50	84	-1.62	0.047
9.250	0.50	172	-1.31	0.033
9.750	0.50	320	-1.04	0.024
10.125	0.25	298	-0.766	0.025
10.375	0.25	439	-0.598	0.021
10.625	0.25	635	-0.438	0.017
10.875	0.25	872	-0.300	0.015
11.125	0.25	1263	-0.141	0.012

Note. — There are N galaxies in each bin centered at K_s and of width ΔK_s , corresponding to number counts of dN/dm in mag⁻¹ deg⁻² and its corresponding Poisson uncertainty. These are the 2MASS $\mu_{K_s} = 20$ mag/arcsec² circular isophotal magnitudes (Jarrett et al. 2000a).